Supplementary Information

Ultrasound-responsive theranostic platform for the timely monitoring and efficient thrombolysis in thrombi of tPA resistance

Lin Lin[1,2,3#], Zhaojing Ba[1#], Hao Tian[1#], Haoxiang Qin[1#], Xi Chen[4], Xin Zhou[1], Shanlan Zhao[1], Lang Li[1], Fangchao Xue[1], Hong Li[5], Lang He[1,3], Xiaochen Li[1], Jiahui Du[1], Zhenhua Zhou[4*], Wen Zeng[1,3,6*]

[1] Department of Cell Biology, Third Military Medical University, Chongqing, China.
[2] School of Medicine, Chongqing University, Chongqing, China.
[3] Chongqing Institute of Advanced Pathology, Jinfeng Laboratory, Chongqing, China.
[4] Department of Neurology, Southwest Hospital, Third Military Medical University, Chongqing, China.
[5] Department of Anesthesiology, Xinqiao Hospital, Third Military Medical University, Chongqing, China.
[6] State Key Laboratory of Trauma, Burn and Combined Injury, Southwest Hospital, Third Military Medical University, Chongqing, China.
*Correspondence: Zhenhua Zhou exploiter001@126.com; Wen Zeng zengw0105@163.com
[#]These authors have contributed equally to this work

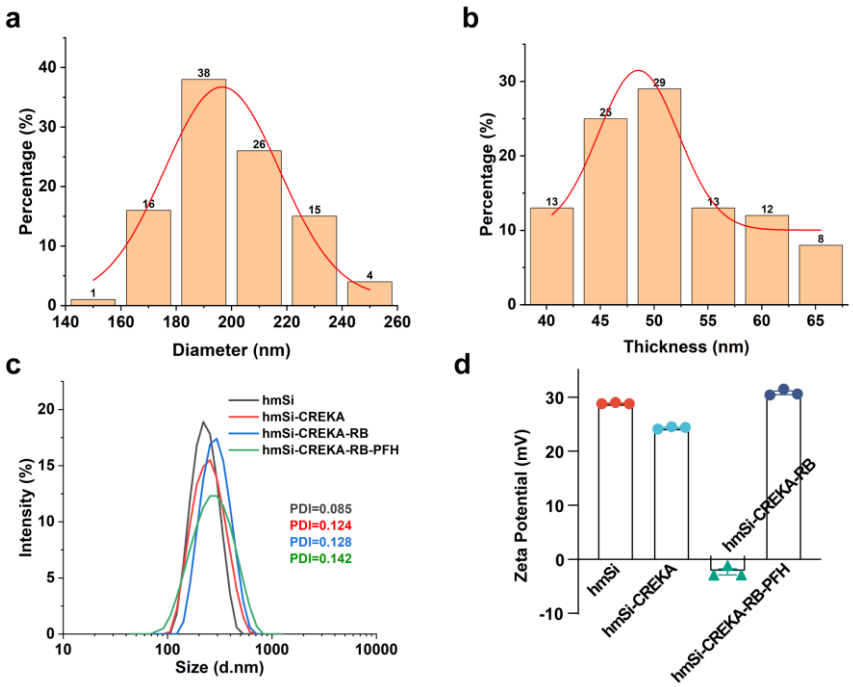

Figure S1. Characterization of hmSi-CREKA-RB-PFH. a Diameter and **b** Thickness of hmSi. **c** Intensity distribution of DLS and **d** ζ potentials of hmSi, hmSi-CREKA, hmSi-CREKA-RB and hmSi-CREKA-RB-PFH. Data are presented as mean±SEM. Source data underlying graph **a-d** are provided as a Source Data file. Each experiment was repeated three times or more independently with similar results.

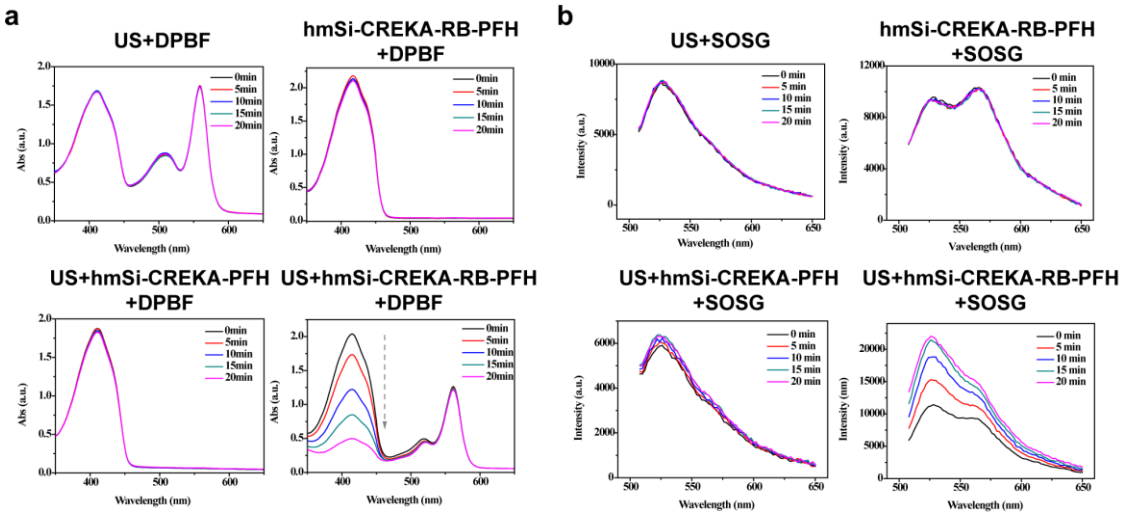

Figure S2. Detection of singlet oxygen generation. Spectral changes of singlet oxygen probe **a** DPBF and **b** SOSG under different treatment conditions. Source data underlying graph **a** and **b** are provided as a Source Data file. Each experiment was repeated three times or more independently with similar results.

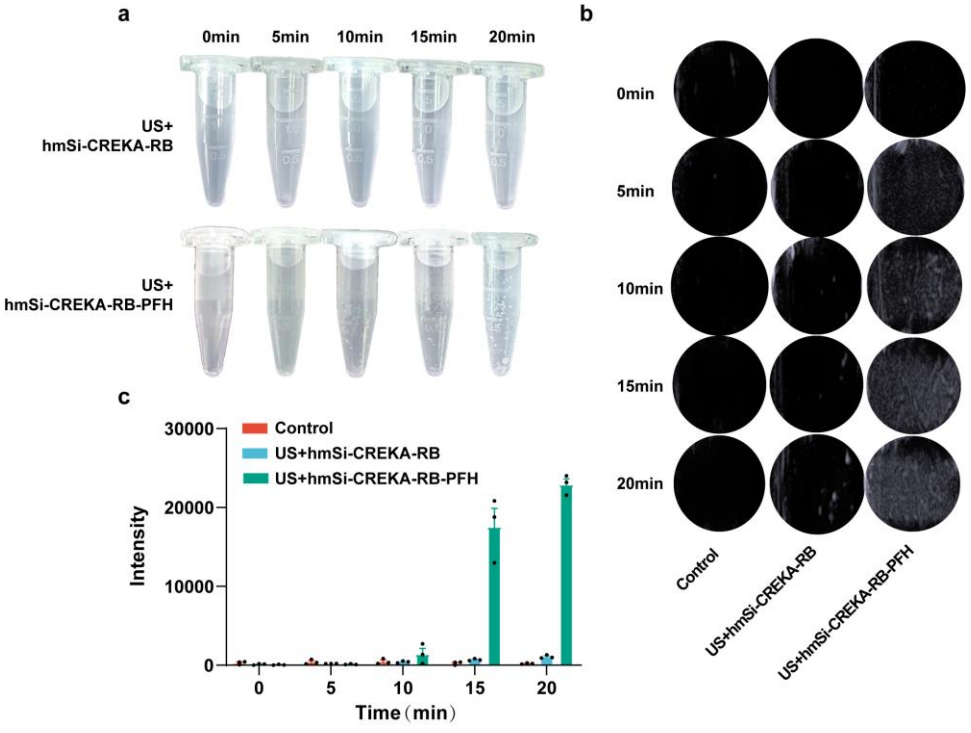

Figure S3. Phase transition of PFH. **a** Digital photos of the US-mediated phase transition of PFH. **b** Resolution improvement of hmSi-CREKA-RB-PFH under ultrasound irradiation. **c** Signal of ultrasound images. n=3 independent experiments. Data are presented as mean±SEM. Source data underlying graph **c** is provided as a Source Data file. Each experiment was repeated three times or more independently with similar results.

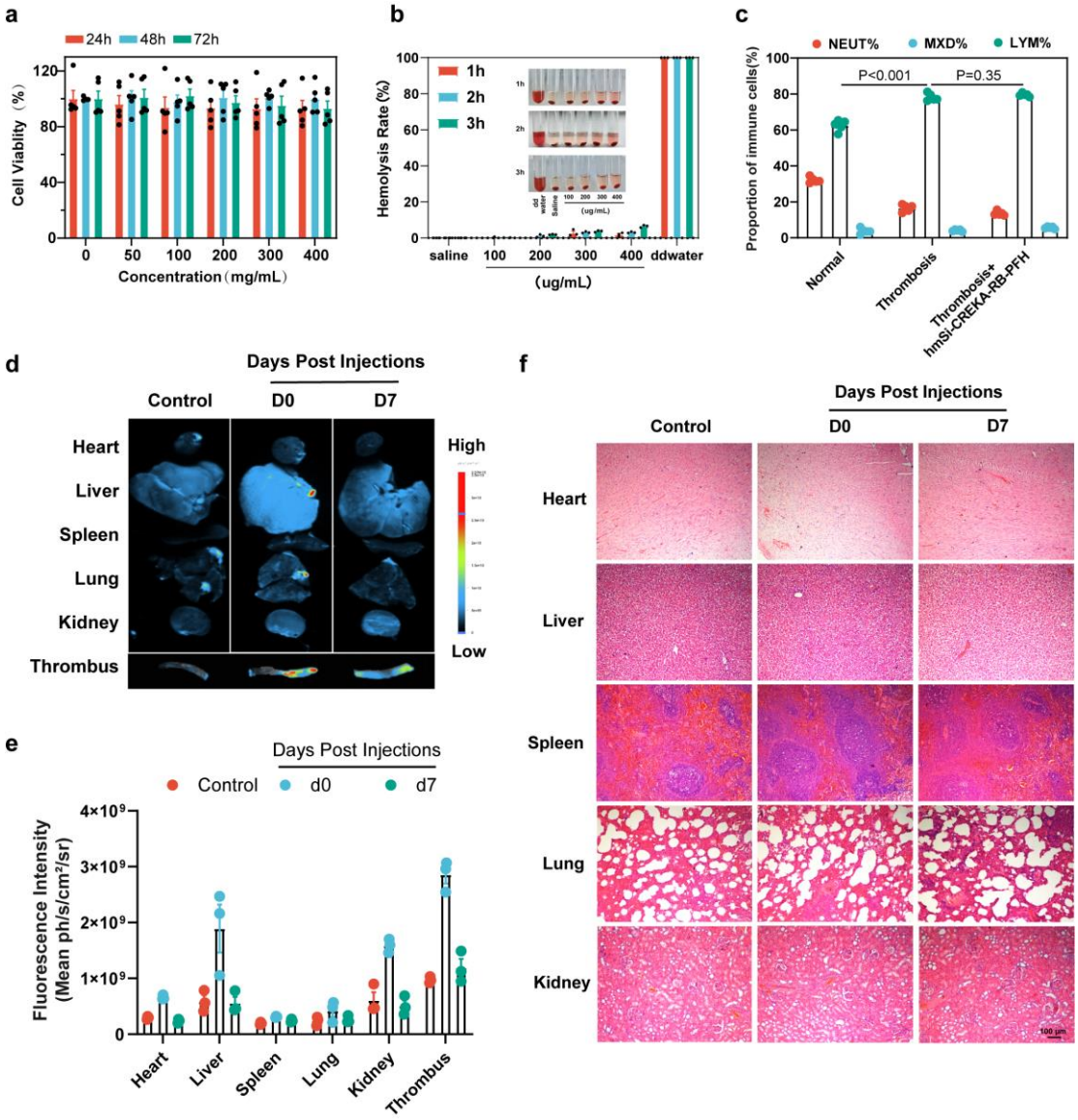

Figure S4. Biosafety of hmSi-CREKA-RB-PFH. a Cytotoxicity of hmSi-CREKA-RB-PFH with different concentrations through CCK8 detection kit. n=5 independent experiments. **b** Hemolysis rate of RBC after incubated with distilled water (positive control), saline (negative control), and hmSi-CREKA-RB-PFH of different concentrations for 1, 2, and 3 h, respectively (inset: Photographs of RBCs in different groups). n=3 independent experiments. **c** Changes of immune cells after hmSi-CREKA-RB-PFH injection. n=5 samples. One way ANOVA with LSD post hoc analysis was employed to compare the differences between groups. **d** Ex vivo fluorescence images and **e** fluorescence intensity of major organs and blocked vessels with hmSi-CREKA(FITC)-RB-PFH injection for three successive days. n=3 samples. **f** H&E staining of major organs with hmSi-CREKA(FITC)-RB-PFH injection for three successive days. Data are presented as mean±SEM. Source data underlying graph **a-c** and **e** are provided as a Source Data file. Each experiment was repeated three times or more independently with similar results.

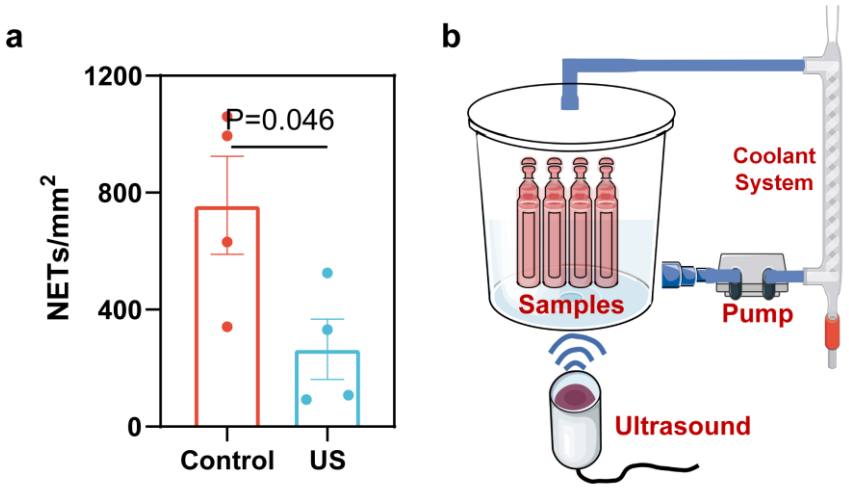

Figure S5. Removal of thermal effect. a Quantification of NETs/mm^2 in clinical thrombi. n=4 samples. Two-tailed independent samples t-test. **b** Schematic diagram of extracorporeal circulation device. Data are presented as mean ± SEM. Source data underlying graph **a** is provided as a Source Data file.

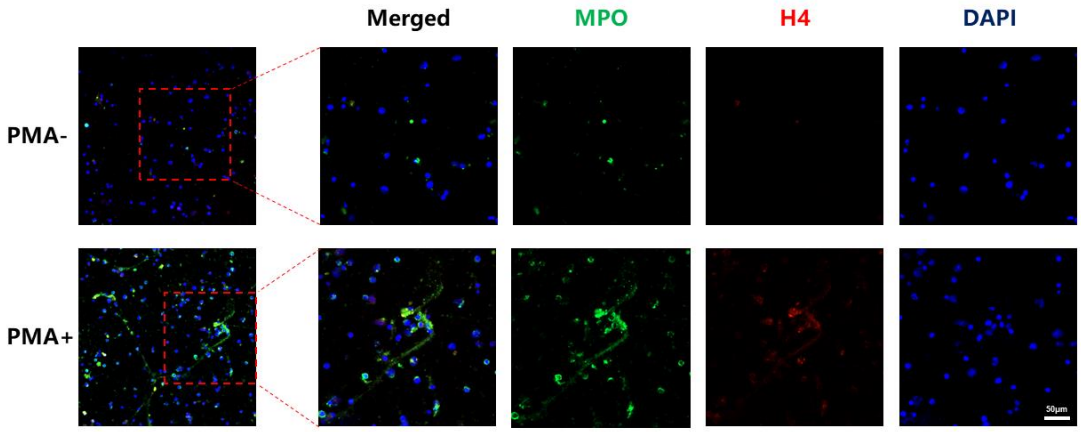

Figure S6. NETs formation in vitro. Neutrophils were treated with PMA to induce NETs and the immunofluorescence staining of NETs. The experiment was repeated more than three times independently with similar results.

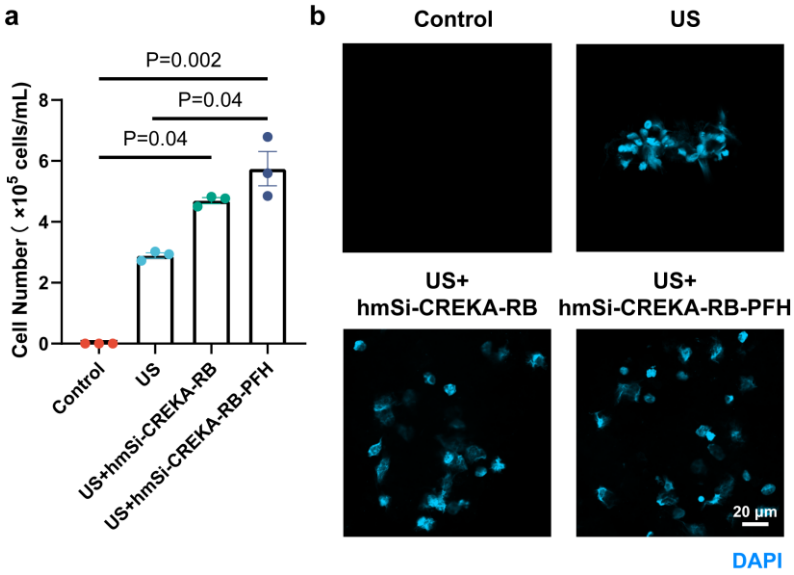

Figure S7. Examination of the shed cells from NETs. a Cell counting of the culture medium after different treatments. n=3 independent experiments. Kruskal-Wallis test was employed to compare the differences between groups. **b** Immunofluorescence staining of the shed cells. Data are presented as mean±SEM. Source data underlying graph **a** is provided as a Source Data file. Each experiment was repeated three times or more independently with similar results.

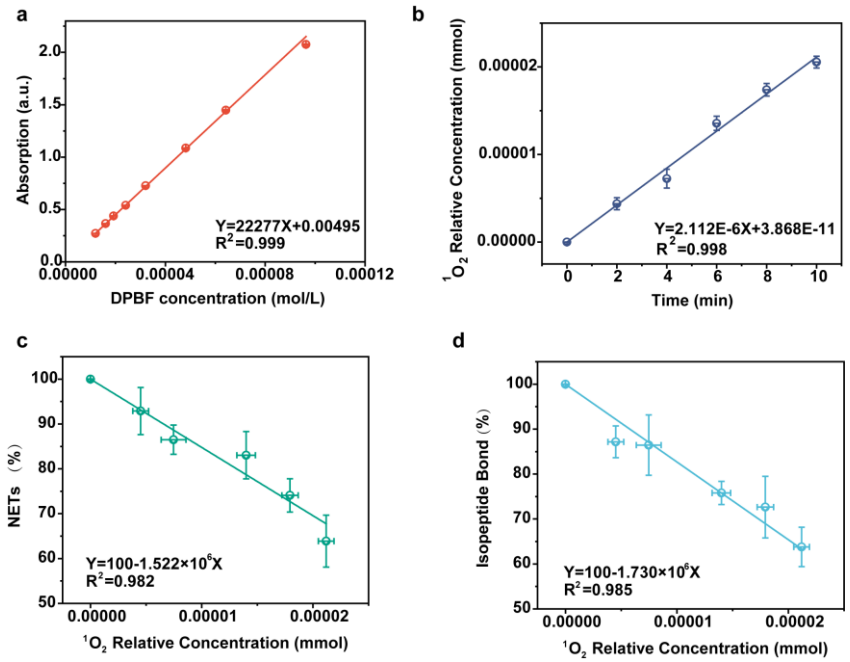

Figure S8. Dose-effect relationship between $^1O_2$ and the content of NETs and isopeptide bonds. a Standard curves of DPBF with different concentrations. **b** The generation of $^1O_2$ along with ultrasonic time. The content changes of **c** NETs and **d** isopeptide bonds under SDT therapy. Data are presented as mean±SEM. Error bars represent standard deviation of three independent experiments. Source data underlying graph **a-d** are provided as a Source Data file.

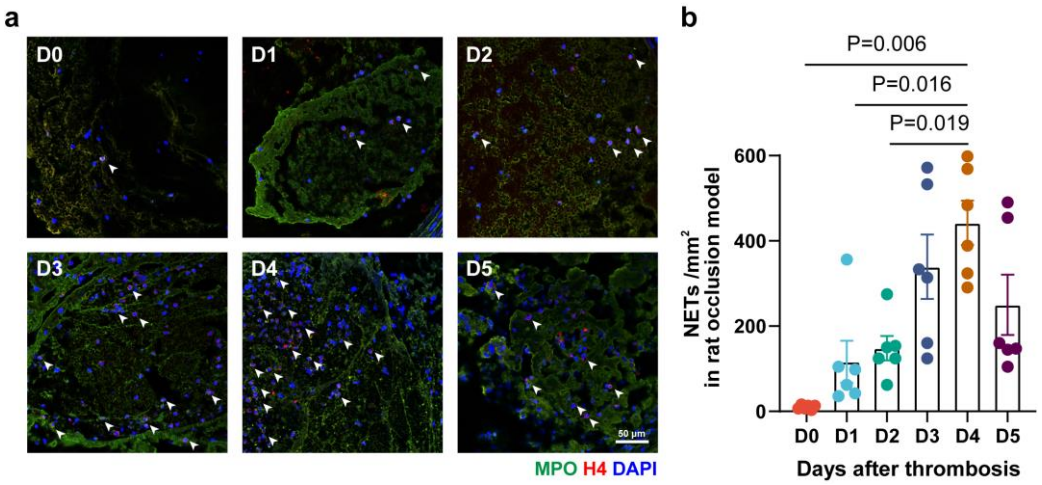

Figure S9. NETs formation in vivo. a The immunofluorescence staining of NETs in rat common carotid artery from D0 to D5 after thrombosis and **b** The number of NETs at different time points. n=6 samples. Data are presented as mean±SEM. Welch's ANOVA with Tamhane's T2 post hoc analysis was employed to compare the differences between groups. Source data underlying graph **b** is provided as a Source Data file.

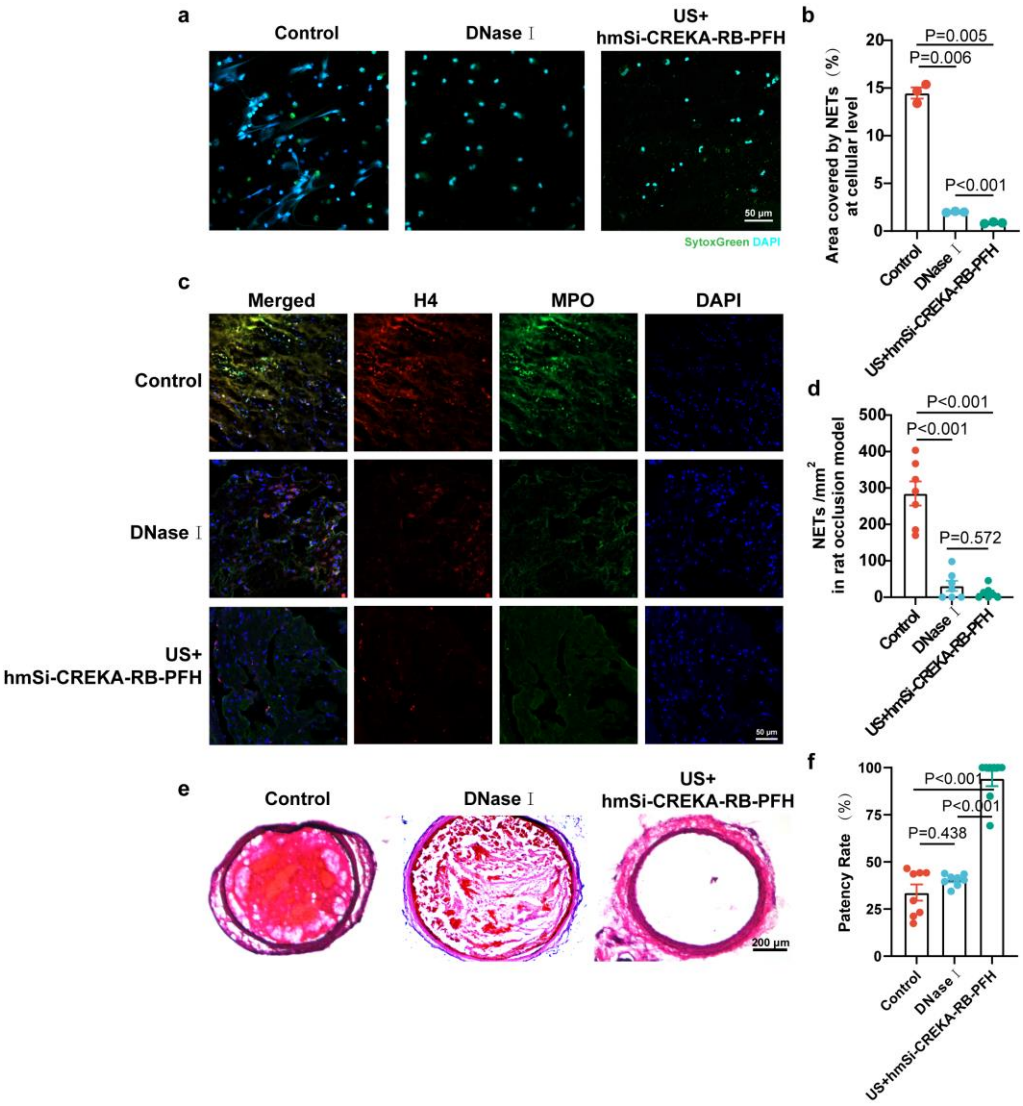

Figure S10. **Therapeutic effect of DNase Ⅰ. a** Immunofluorescence staining of NETs induced in vitro and **b** the area covered by NETs after different treatments, n=3 independent experiments. **c** Immunofluorescence staining of NETs in rat occlusion model and **d** Quantification of NETs/mm^2 after different treatments, n=8 samples. **e** H&E staining and **f** its corresponding patency rate, n=8 samples. Data are presented as mean±SEM. Welch's ANOVA with Tamhane's T2 post hoc analysis was employed to compare the differences between groups. Source data underlying graph **b, d** and **f** are provided as a Source Data file.

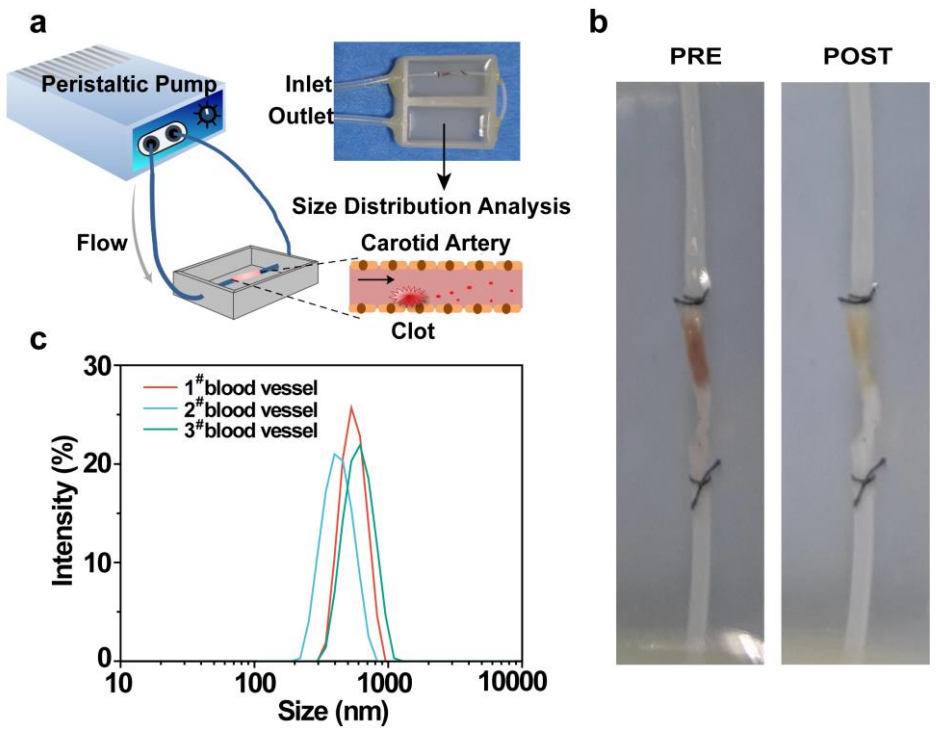

Figure S11. Ex vivo scouring of US+hmSi-CREKA-RB-PFH treated-vessel. a Schematic diagram of in-vitro analog of shear stress. **b** Photograph of the rat carotid artery blood vessels with incomplete patency before and after washed in vitro. **c** Size distribution analysis of the collected supernatants of rat carotid artery blood vessel. Source data underlying graph **c** is provided as a Source Data file. Each experiment was repeated three times or more independently with similar results.

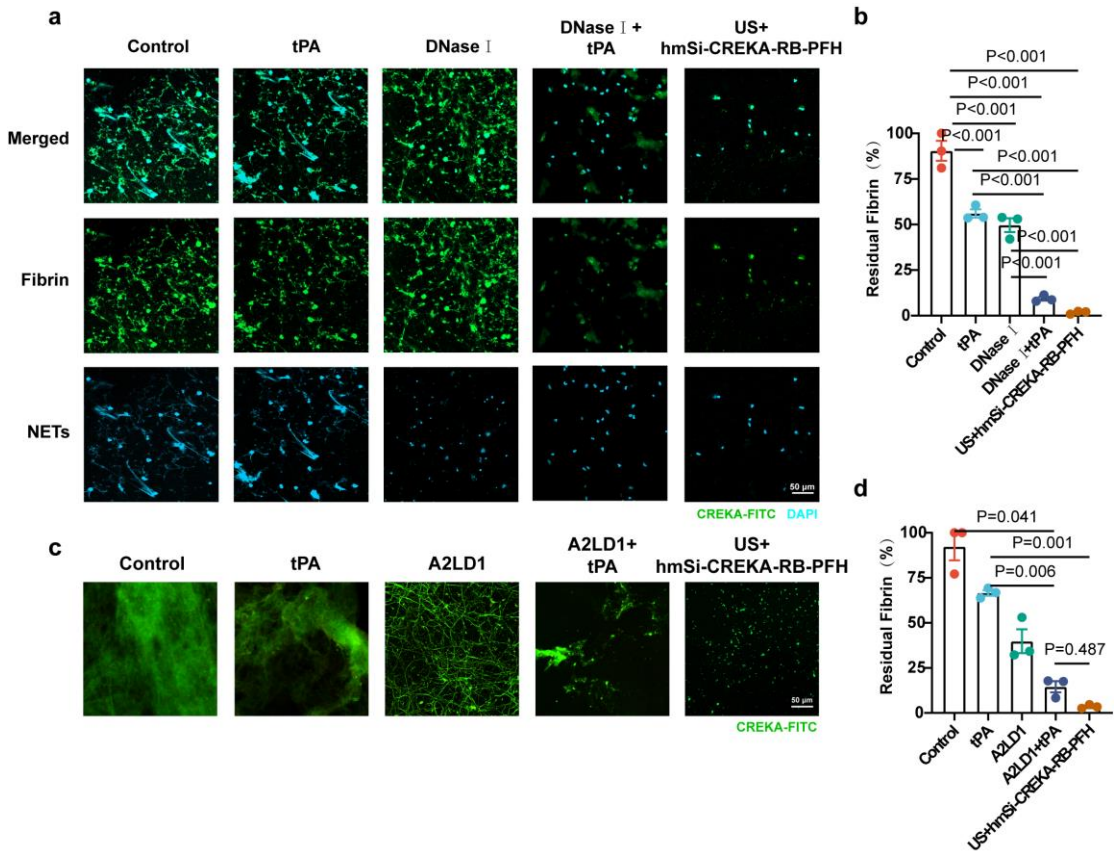

Figure S12. Relationship between disruption of NETs and isopeptide bonds and promotion of fibrin degradation. a Complex of NETs and fibrin under different treatments and **b** the residual fibrin after treatments, n=3 independent experiments. One way ANOVA with LSD post hoc analysis was employed to compare the differences between groups. **c** Fibrin network under different treatments and **d** the residual fibrin after treatments, n=3 independent experiments. Welch's ANOVA with Tamhane's T2 post hoc analysis was employed to compare the differences between groups. Data are presented as mean ± SEM. Source data underlying graph **b** and **d** are provided as a Source Data file. Each experiment was repeated three times or more independently with similar results.

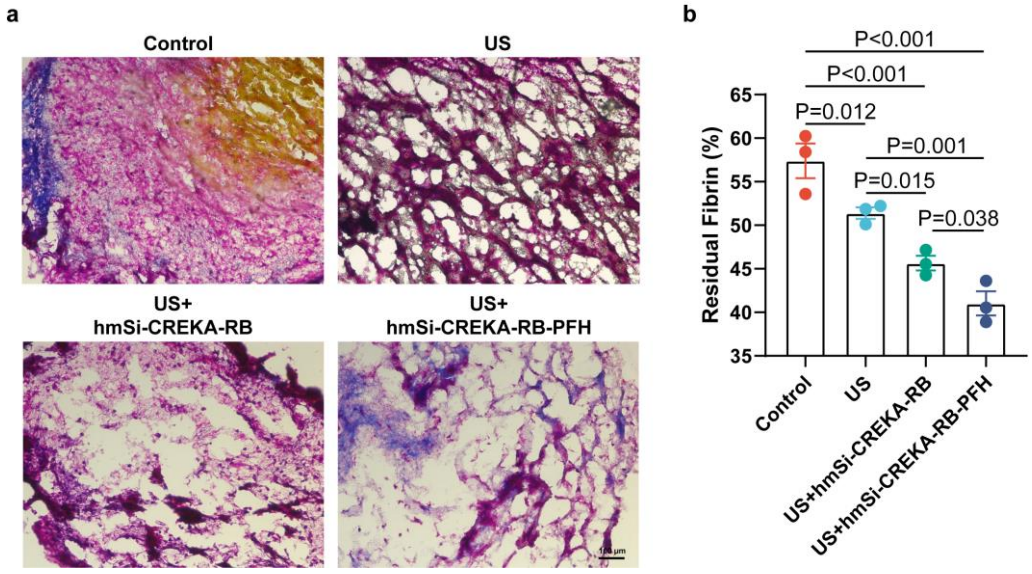

Figure S13. MSB staining of clinical thrombi under different treatment. a MSB staining and **b** the area of residual fibrin, n=3 samples. MSB, Methyl Green-Pyronin Y-Saffron. Data are presented as mean ± SEM. One way ANOVA with LSD post hoc analysis was employed to compare the differences between groups. Source data underlying graph **b** is provided as a Source Data file.

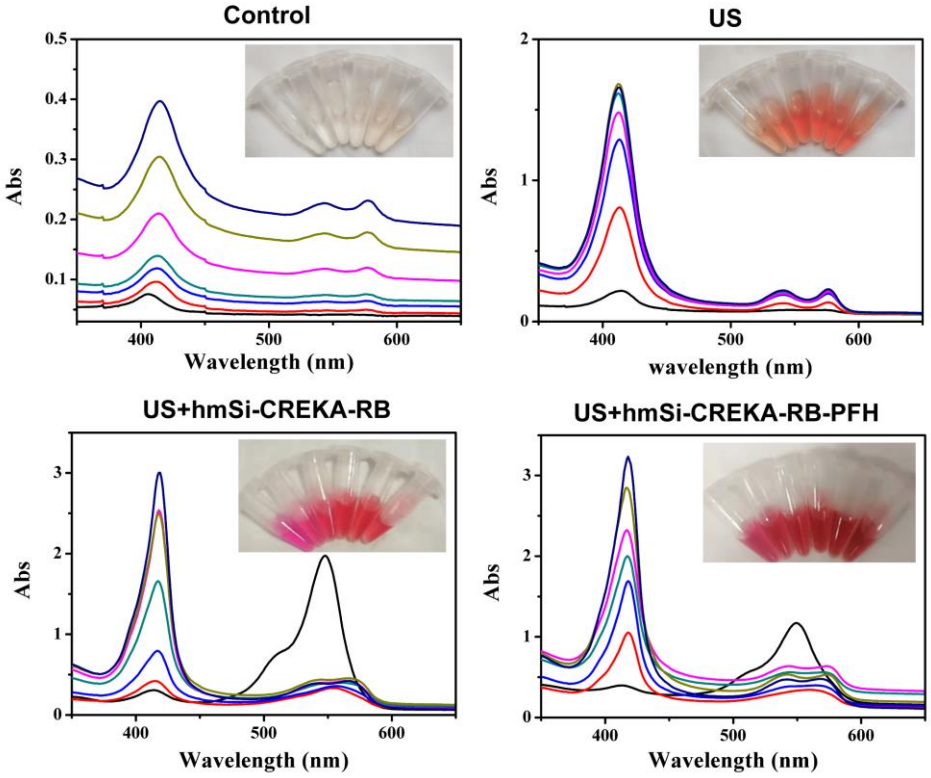

Figure S14. UV-vis detection of the breakdown of fibrin scaffold. UV absorption peaks of supernatant at 405nm of artificial thrombus at different conditions. Each experiment was repeated three times or more independently with similar results.

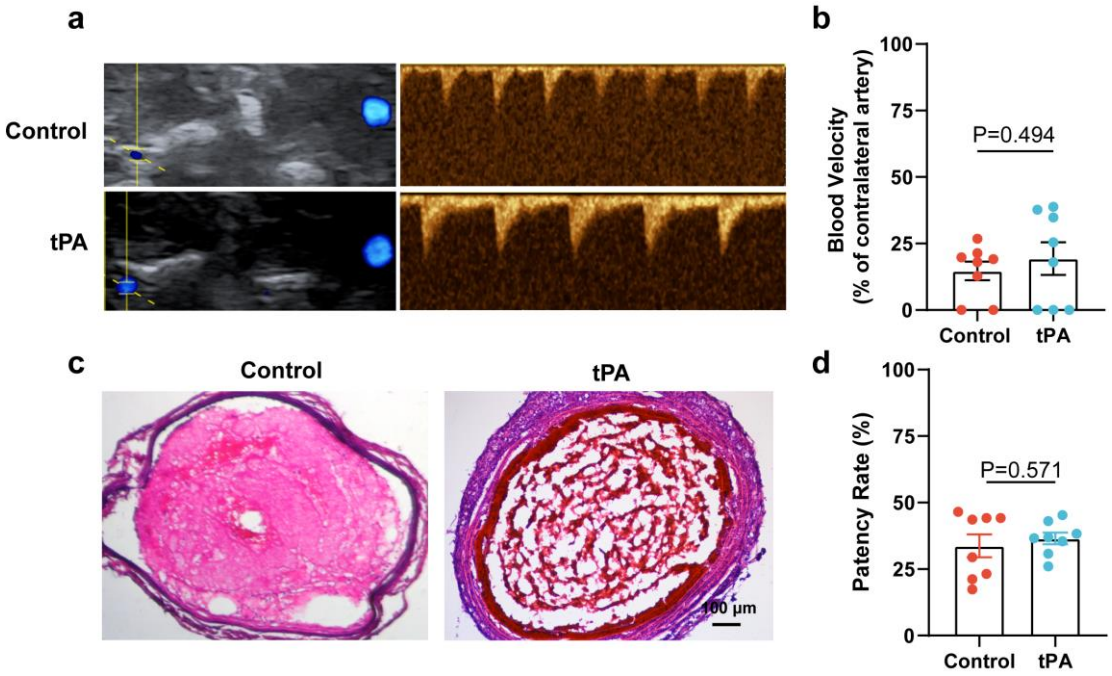

Figure S15. **Therapeutic effect of tPA in rat occlusion model. a** Doppler ultrasound and **b** blood velocity of tPA-treated vessels, n = 8 samples. Two-tailed paired samples t-test was employed to compare the differences between groups. **c** H&E staining and **d** the corresponding patency rate after treatment. n = 8 samples. Two-tailed independent samples t-test was employed to compare the differences between groups. Data are presented as mean±SEM. Source data underlying graph **b** and **d** is provided as a Source Data file.

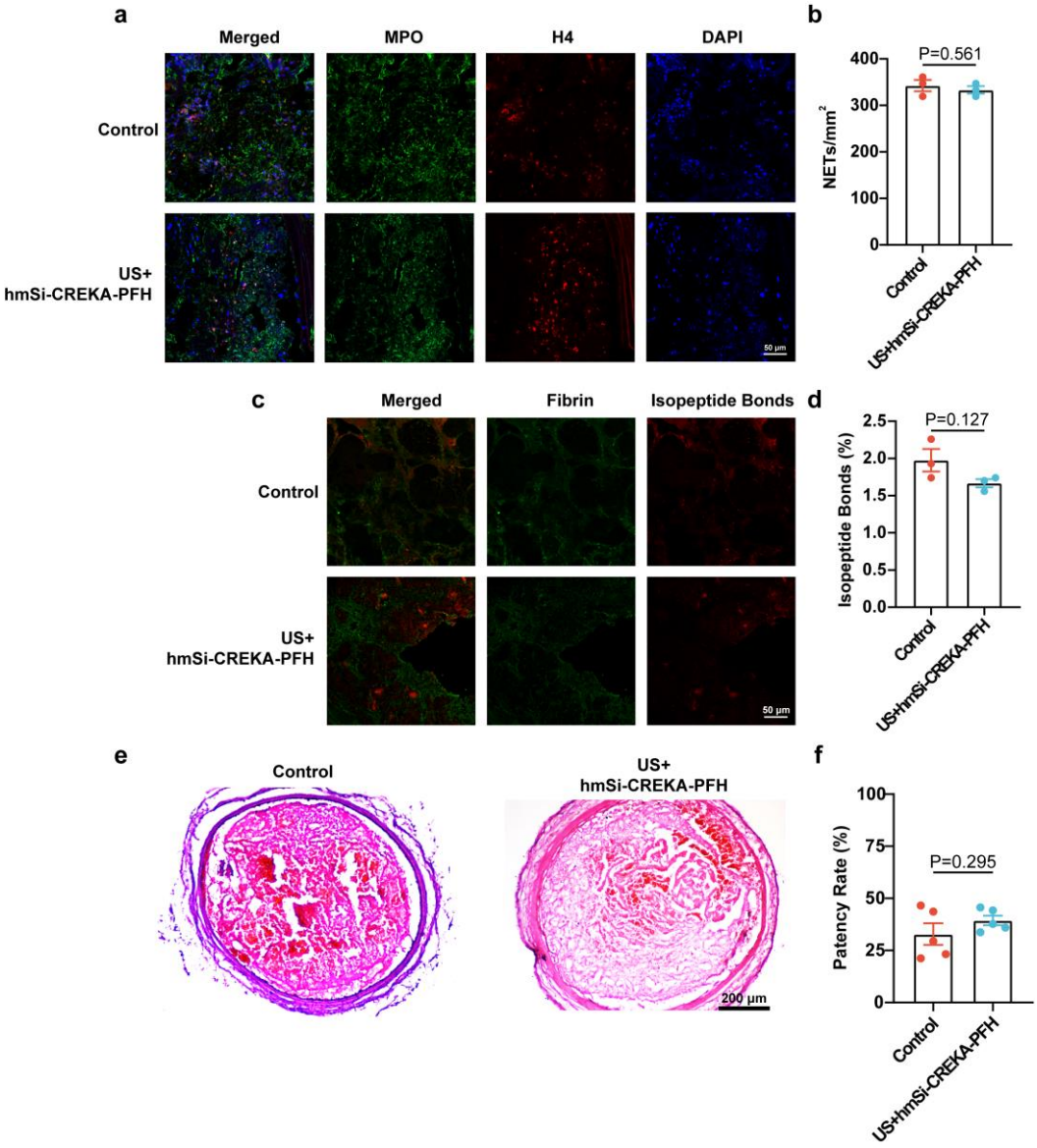

Figure S16. Therapeutic effect of US + hmSi-CREKA-PFH. a Immunofluorescence staining of NETs in control and US+hmSi-CREKA-PFH groups in rat occlusion model. **b** Statistics of NETs per unit area. n=3 samples. **c** Immunofluorescence staining of isopeptide bonds in control and US+hmSi-CREKA-PFH groups in rat occlusion model. **d** Statistics of isopeptide bonds. n=3 samples. **e** H&E staining and **f** the corresponding patency rate. n=5 samples. Data are presented as mean±SEM. Two-tailed independent samples t-test was employed to compare the differences between groups. Source data underlying graph **b, d** and **f** are provided as a Source Data file.

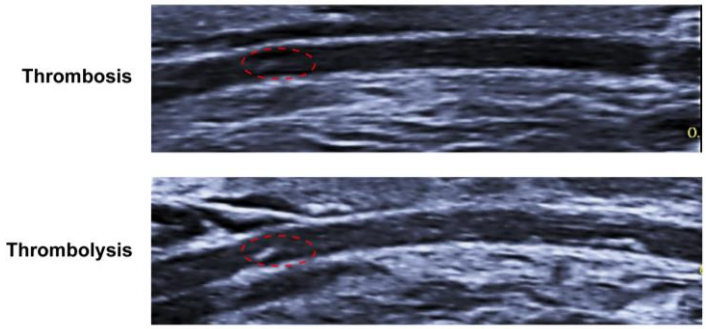

Figure S17. **The contrast-enhancement ultrasound imaging of rats.** With the progress of ultrasound therapy, the morphology of intravascular thrombosis gradually became clear. The experiment was repeated more than three times independently with similar results.

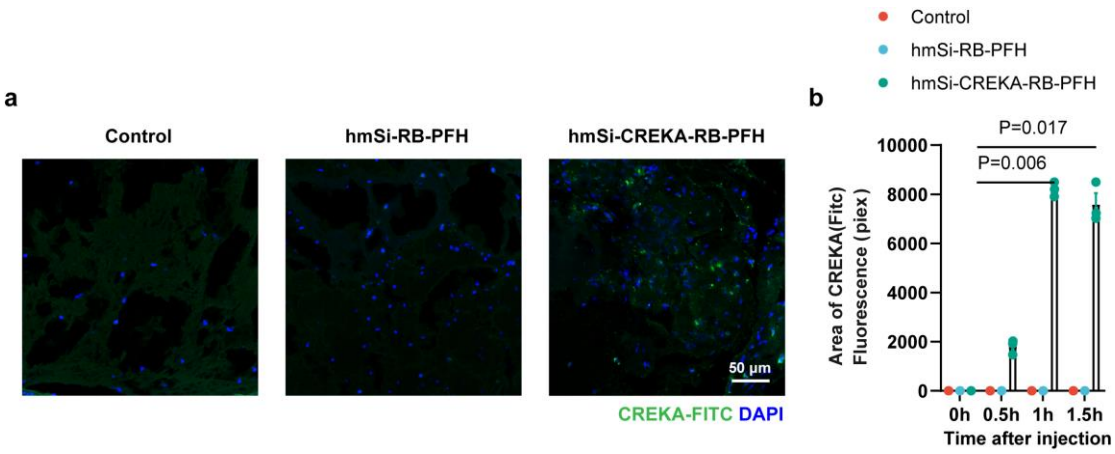

Figure S18. The thrombus-targeting ability of hmSi-CREKA(FITC)-RB-PFH. a Fluorescence images and **b** Statistics of fluorescence area after different injection time. n=3 samples. Data are presented as mean±SEM. Source data underlying graph **b** is provided as a Source Data file. Kruskal-Wallis test was employed to compare the differences between groups.

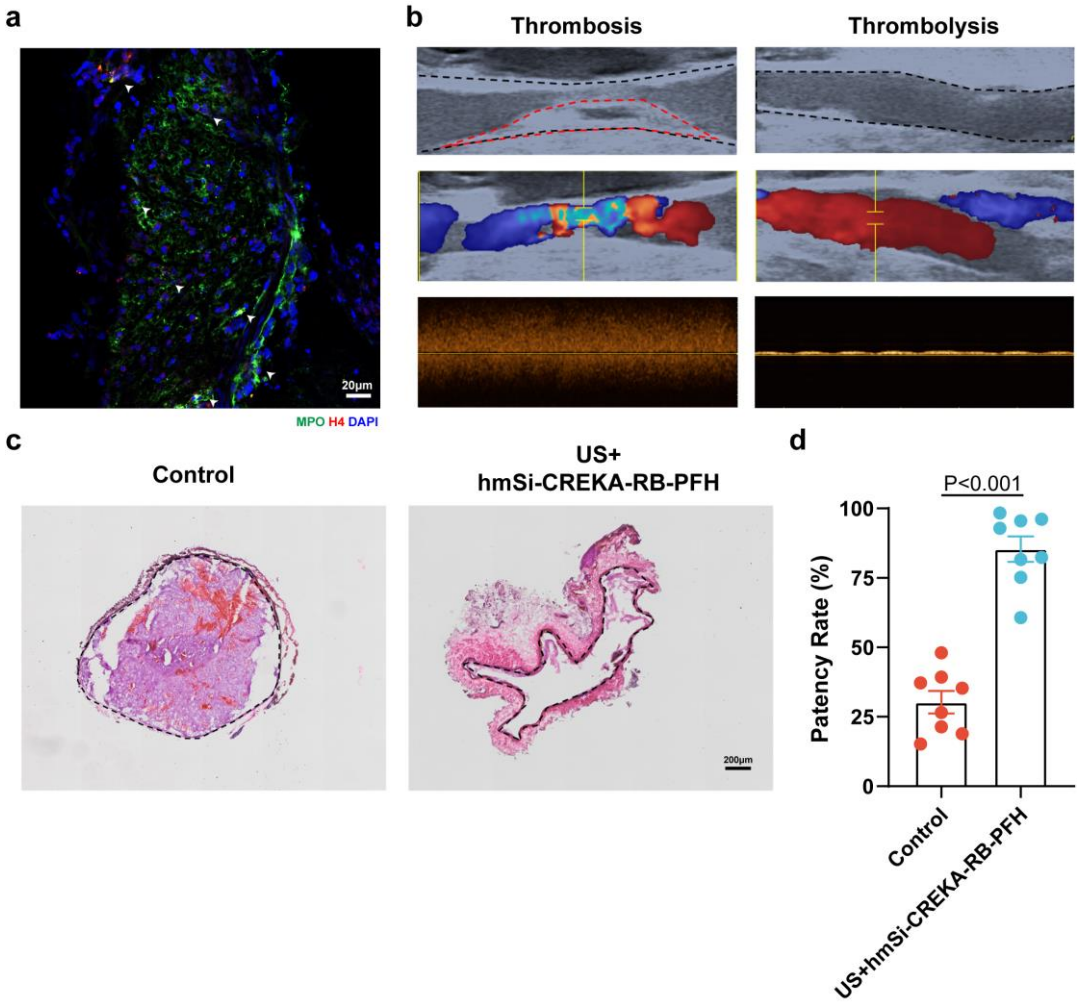

Figure S19. **Therapeutic effect of US+hmSi-CREKA-RB-PFH on IVC model. a** Immunofluorescence of NETs in IVC thrombus. **b** Doppler ultrasonography of IVC vessels before and after treatment. **c** H&E staining and **d** the patency rate of IVC vessels. n=8 samples. Data are presented as mean±SEM. Two-tailed independent samples t-test was employed to compare the differences between groups. Source data underlying graph **d** is provided as a Source Data file. Each experiment was repeated three times or more independently with similar results.

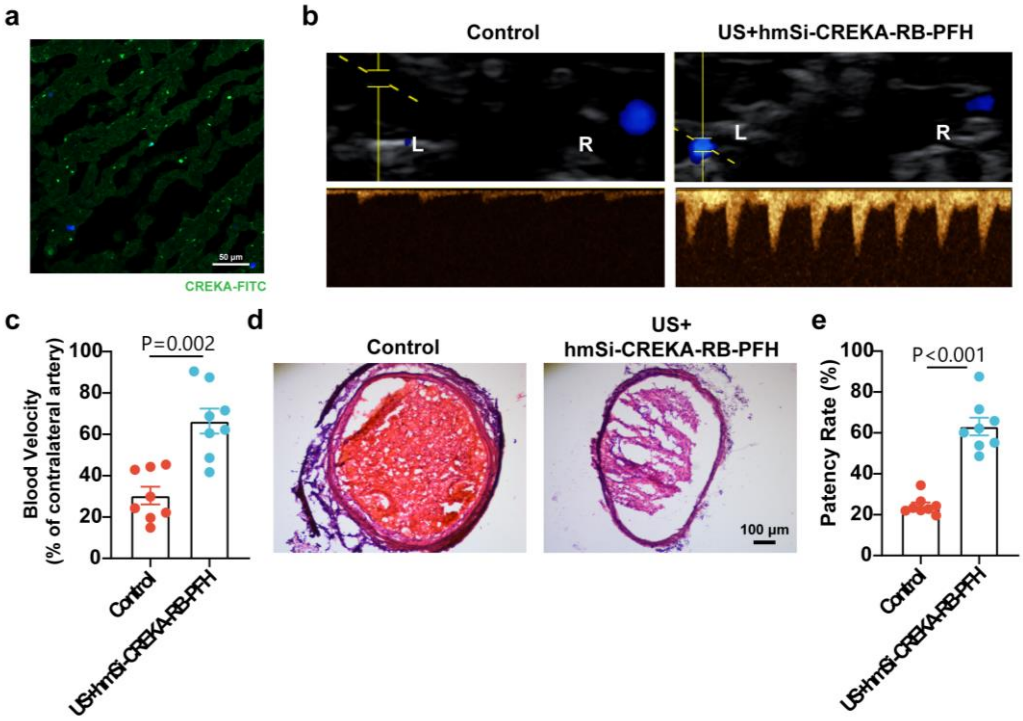

Figure S20. The therapeutic effect of US+hmSi-CREKA-RB-PFH in rat old thrombi. a Targeting ability of hmSi-CREKA-RB-PFH to old thrombi. **b** Real time Doppler ultrasound and **c** blood velocity in one-month occlusion model. n = 8 samples. Two-tailed paired samples t-test was employed to compare the differences between groups. **d** H&E staining and **e** the corresponding patency rate. n=8 samples. Two-tailed independent samples t-test was employed to compare the differences between groups. Data are presented as mean±SEM. Source data underlying graph **c** and **e** is provided as a Source Data file. Each experiment was repeated three times or more independently with similar results.

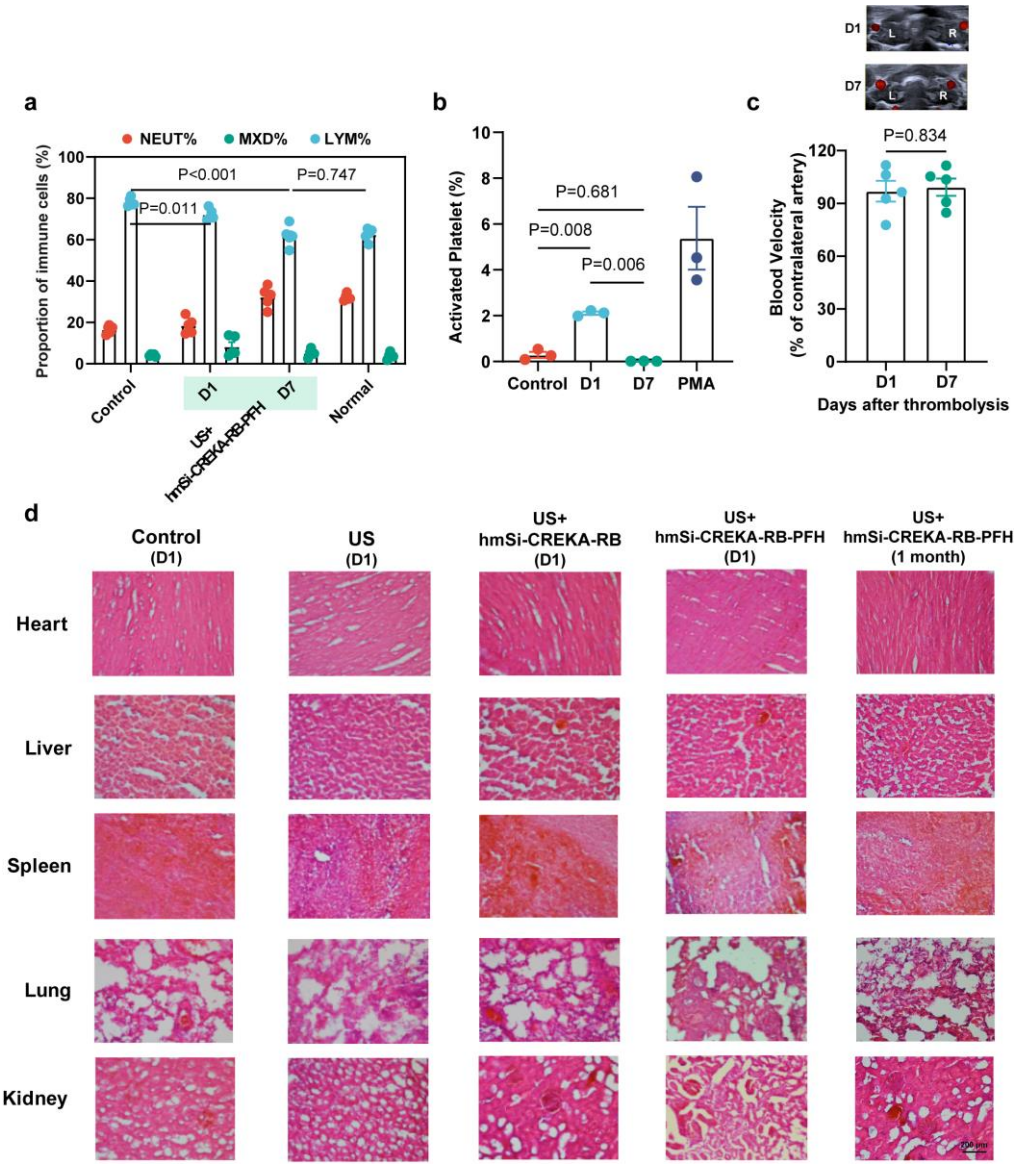

Figure S21. Safety assessment after treatment. a Proportion of immune cells in the blood of rats with different treatment (D1 and D7 means the first and seventh day after completing three consecutive days of treatment,respectively). n=5 samples. NEUT%,neutrophil%. MXD%, monocyte%. LYM%, lymphocyte%. one-way ANOVA with the LSD post hoc test was employed to compare the differences between groups. **b** Platelet activation rate in different time after treated with US+hmSi-CREKA-RB-PFH. n=3 samples. Welch's ANOVA with Tamhane's T2 post hoc analysis was employed to compare the differences between groups. **c** Doppler ultrasound and the relative patency rate of the recanalized vessels. n = 5 samples, Two-tailed paired samples t-test was employed to compare the differences between groups. **d** H&E staining of major organs after different treatments. Data are presented as mean±SEM. Source data underlying graph **a-c** are provided as a Source Data file. Each experiment was repeated three times or more independently with similar results.

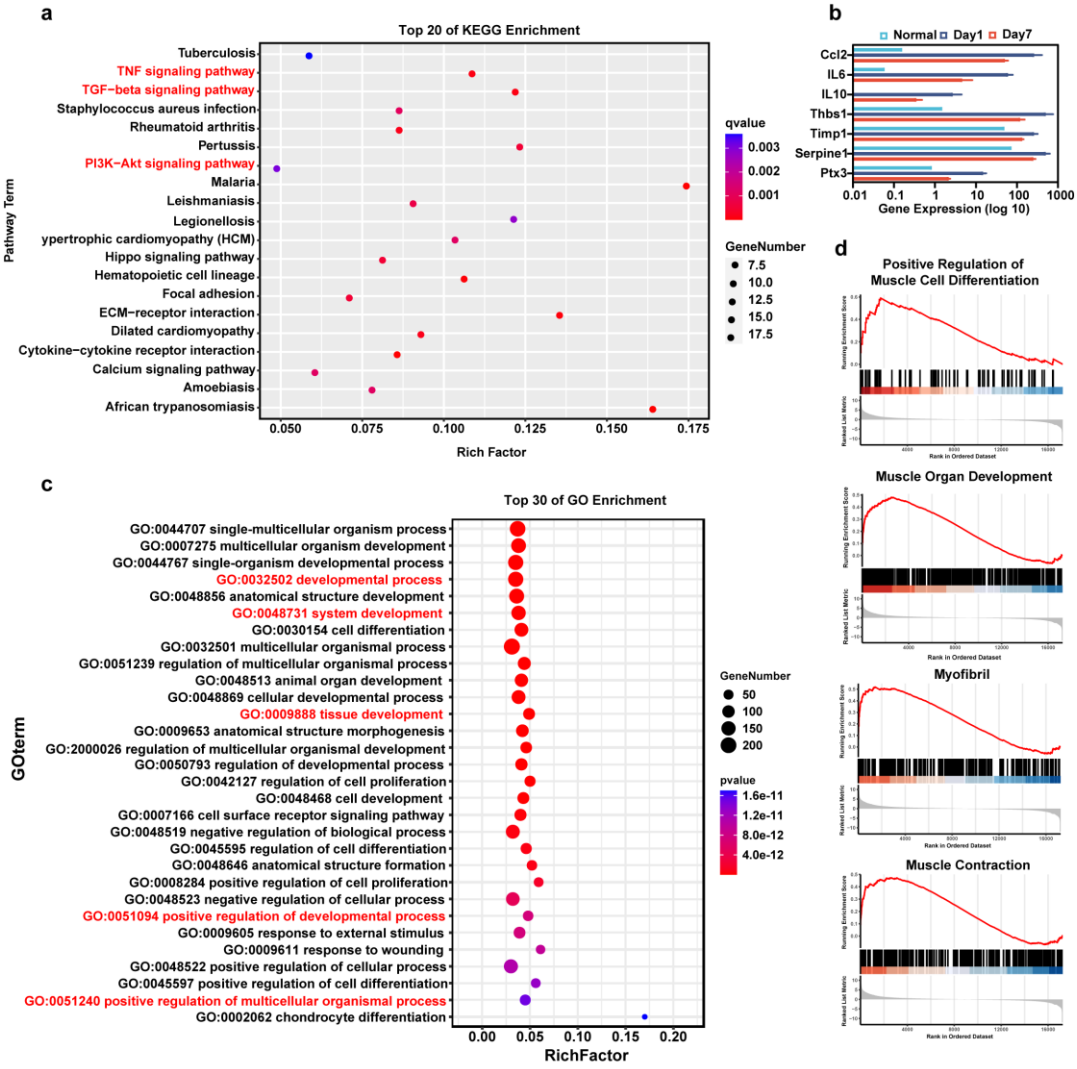

Figure S22. Bulk RNA sequencing of the recanalized vessels. a Top 20 most significantly regulated KEGG pathways a day and a week after combination therapy. (|fold-change| ⩾ 1.0 with P value < 0.05). **b** Changes of inflammation-related Ccl2,IL6,IL10 and homeostasis-related Thbs1,Timp1,Serpine1 and Ptx3 a day and a week after combination therapy. n=3 samples. Data are presented as mean±SEM. **c** Top 30 most significantly regulated GO biological process enrichment between the two groups (P<0.05 and |log2 FC|>1). **d** GSEA analysis of muscle cell differentiation, muscle organ development,myofibril and muscle contraction. Source data underlying graph **b** is provided as a Source Data file.

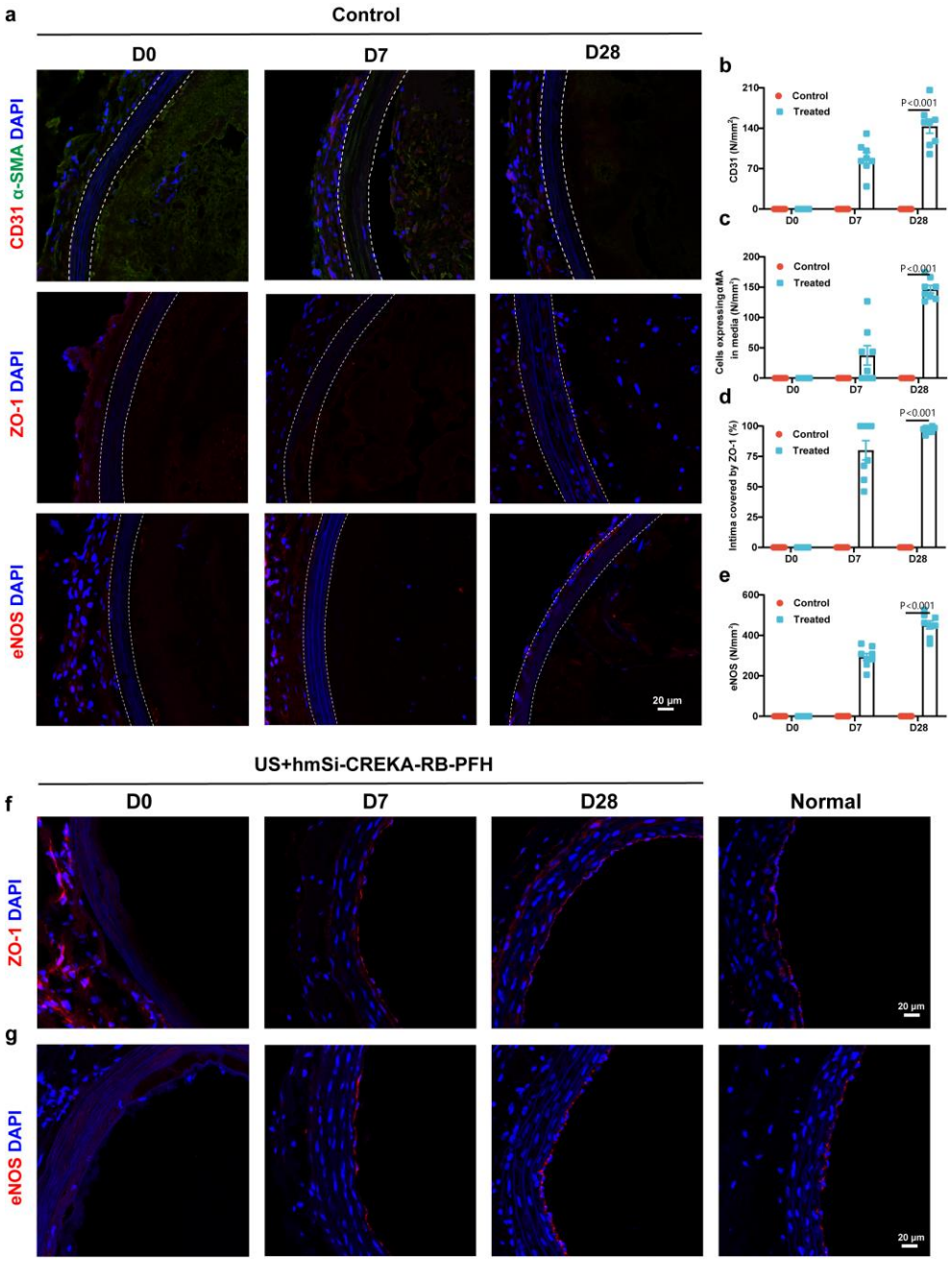

Figure S23. Vascular remodeling. a Immunofluorescence staining of CD31,α-SMA,ZO-1 and eNOS in untreated control blood vessels and the quantification of **b** CD31 **c** α-SMA **d** ZO-1 and **e** eNOS. n=8 samples. Immunofluorescence staining of **f** ZO-1 and **g** eNOS in combination treated blood vessels. Data are presented as mean ± SEM. Two-tailed independent samples t-test was employed to compare the differences between groups. Source data underlying graph **b-e** are provided as a Source Data file. Each experiment was repeated three times or more independently with similar results.

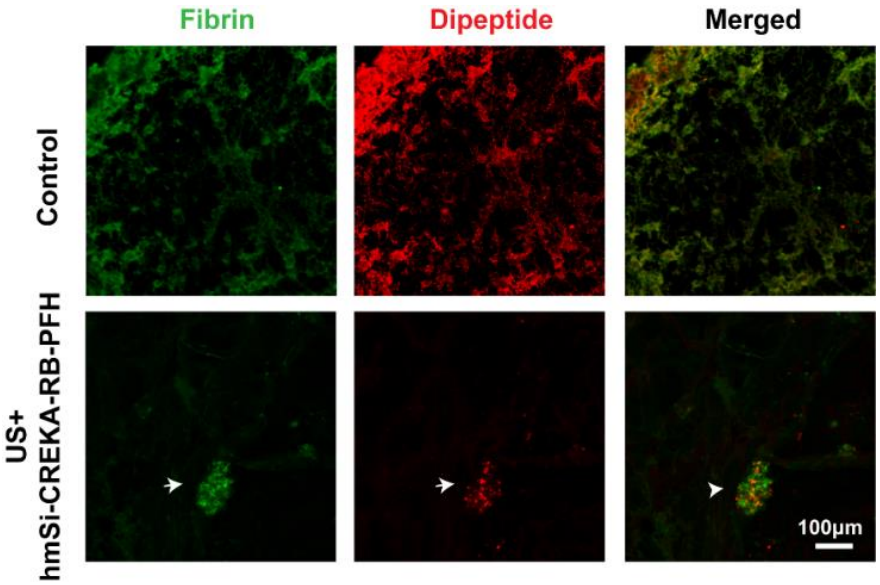

Figure S24. Immunofluorescence staining of isopeptides. In pig femoral artery thrombus model, after 30 minutes' treatment, the vessel was taken out for immunofluorescence staining.

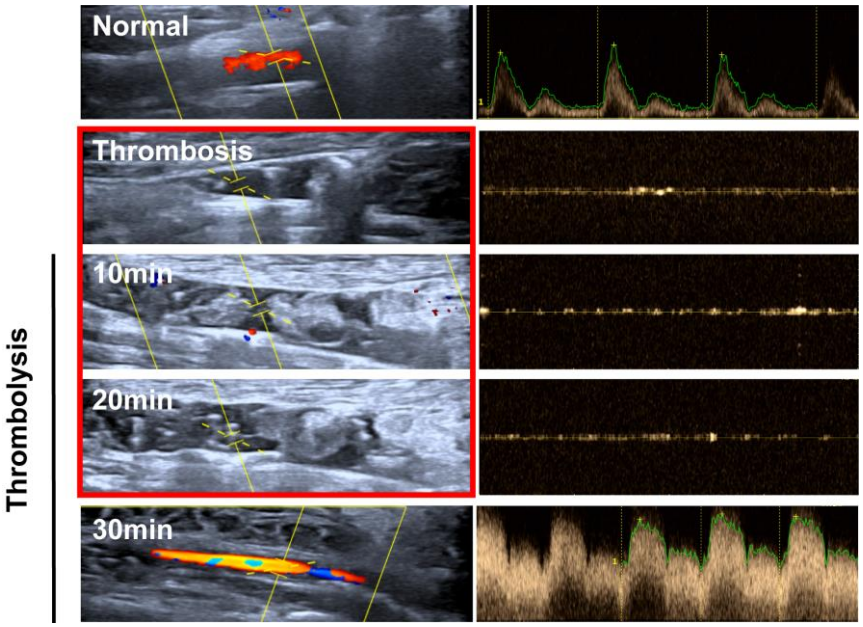

Figure S25. Contrast-enhancement in pig carotid artery. Ultrasound imaging during the treatment of femoral artery thrombosis in pigs.